



POLITECNICO
MILANO 1863

SCUOLA DI INGEGNERIA INDUSTRIALE
E DELL'INFORMAZIONE

Modeling Hydrogen Production in Dark Fermentation: Analyzing the Impact of Homoacetogenesis Pathway

TESI DI LAUREA MAGISTRALE IN
CHEMICAL ENGINEERING
INGEGNERIA CHIMICA

Author: **Lucia Romano**

Student ID: 10628259

Advisor: Giulia Bozzano

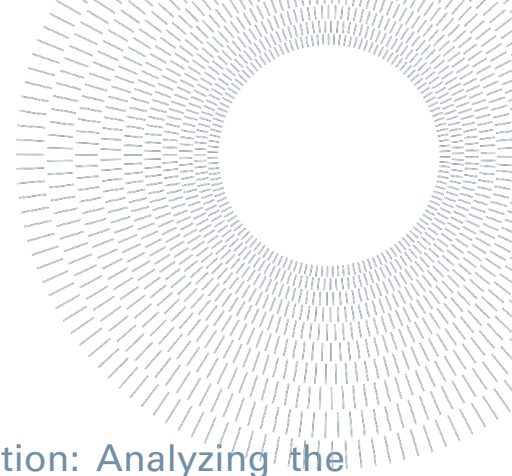
Co-advisor: Federico Moretta

Academic Year: 2023-24



POLITECNICO
MILANO 1863

SCUOLA DI INGEGNERIA INDUSTRIALE
E DELL'INFORMAZIONE



Modeling Hydrogen Production in Dark Fermentation: Analyzing the Impact of Homoacetogenesis Pathway

TESI MAGISTRALE IN CHEMICAL ENGINEERING

Romano, Lucia, 10628259

Advisor:

Giulia Bozzano

Co-advisors:

Federico Moretta

Academic year:

2023-24

Abstract: The production of hydrogen through sustainable methods has recently gained increasing attention due to its current and potentially expanding future importance. Dark fermentation (DF) represents a promising yet underexplored approach, largely due to its poor predictability linked to the complexity of microbial metabolic activity. To address this challenge, recent efforts have focused on developing predictive models for DF hydrogen production, with the aim of making the process industrially scalable. This study presents a model incorporating two primary metabolic pathways—acetate and butyrate pathways—along with homoacetogenesis. The model was compared with experimental data coming from five batch cases and one continuous case, with operating conditions varying in volume, pH, duration, and substrate type. The comparison is quite satisfactory. The analysis highlights the growing importance of homoacetogenesis, which showed a stronger impact, particularly in batch operations, where this metabolic pathway was activated earlier in the process.

Key-words: Hydrogen, Dark Fermentation, Homoacetogenesis, Modeling

1. Introduction

The world faces an energy crisis aggravated by the increasing global population[1]. The strong dependence on fossil fuels has caused a climate crisis and led to the gradual depletion of these non-renewable resources[2]. This has resulted in hydrogen emerging as a viable alternative; while having a high energy content of 142 MJ/kg, hydrogen is a clean and renewable fuel that produces only water upon combustion[3].

Hydrogen can be used both for electricity generation and as a component in fuel gas mixtures. In power generation, it sparks fuel cells that convert chemical energy into electricity with high energy efficiency and no greenhouse gas emissions[4]. As a blending gas, hydrogen can be mixed with natural gas and distributed through existing infrastructure, enabling a gradual transition to a more sustainable energy system without the need for immediate investment in new distribution networks[5]. Studies suggest indeed that a blend containing 5–15% hydrogen would necessitate only minimal modifications to the operation and maintenance of current gas networks[6].

Moreover, hydrogen is currently being used across various industrial sectors as an important raw material, further supporting the interest in this field. In the chemical industry, ammonia is the primary application, accounting for more than half of the global hydrogen consumption and the demand for fertilizers is likely to grow to support the increasing need for global food production[7].

The petrochemical industry is responsible for 40% of the world's hydrogen demand, as it employs hydrogen to remove nitrogen and sulfur from coal, improve combustion characteristics, and convert heavy hydrocarbons into higher-value products by increasing the hydrogen-to-carbon ratio[8]19/11/2024 22:39:00. In the metallurgical industry, hydrogen is utilized to eliminate impurities during nickel extraction from nickel sulfate and in the sintering and annealing of metal powders[9]. Furthermore, in the biochemical sector, hydrogen acts as an electron donor and reducing agent for synthesizing compounds such as methane, methanol, acetate, ethanol, and microbial proteins[10].

However, besides its extensive industrial applications and promising prospects for future innovations, hydrogen production currently relies on fossil-derived feedstocks through processes that are unsustainable in the long term and pose significant environmental challenges. In particular, the most prevalent method is steam methane reforming (SMR) accounting for approximately 50% of global hydrogen production[11]. Although economically advantageous -with production costs ranging from \$1.48 to \$2.27 per kilogram - SMR is energy-intensive and contributes significantly to greenhouse gas emissions[12]. Coal gasification represents another major pathway, utilizing abundant coal reserves but similarly imposing considerable environmental burdens, producing hydrogen at costs between \$0.36 and \$1.83 per kilogram[13].

Alternative hydrogen production technologies are therefore being explored to mitigate these environmental impacts. Biomass-derived methods, such as gasification and pyrolysis, present viable routes for hydrogen synthesis and offer competitive cost structures, ranging between \$1.44 and \$2.83 per kilogram[14]. However, their contribution to the overall hydrogen supply remains marginal due to the nascent stage of technological advancements required for large-scale implementation[15].

Water electrolysis emerges as a more sustainable hydrogen production technology, employing electrical energy to dissociate water into hydrogen and oxygen. This method provides environmental advantages by eliminating direct carbon emissions during production[16]. Nevertheless, it is constrained by high operational costs - estimated between \$4.36 and \$7.36 per kilogram of hydrogen - thereby limiting its economic feasibility and widespread adoption[12].

Biological hydrogen production methodologies, including photolysis, photo-fermentation, and dark fermentation, enable hydrogen generation at ambient temperatures using microorganisms as biocatalysts[17]. These bio-based processes offer environmentally benign pathways and provide potential for organic waste valorization. Yet, these processes are currently hindered by low hydrogen yields and require further optimization for scalability and industrial applicability[18]. Furthermore, although these processes are heading in the right direction, they still account for a portion of GHG emissions [19].

Advancing low-carbon hydrogen production technologies is therefore critical given the imperative for sustainable development and the need to reduce greenhouse gas emissions. Transitioning towards renewable-based hydrogen synthesis pathways is essential to facilitate the integration of hydrogen as a cornerstone in the emerging low-carbon economy. Investing in and progressing sustainable hydrogen production technologies would not only allow to address environmental concerns but also reinforce hydrogen's role as a fundamental element in a low-carbon society[20].

Dark fermentation (DF) is a simple, cost-effective, and environmentally friendly biological process for hydrogen production using anaerobic bacteria that employ multi-enzyme systems[21]. Unlike photo-fermentation processes, DF operates independently of light, eliminating a significant technical constraint and enhancing its applicability[22]. Provided ambient conditions and the absence of oxygen, it converts organic compounds - including a wide range of organic and cellulosic wastes such as sludge, leachate, pomace, stalks, and bagasse - into hydrogen. This versatility could contribute to waste recycling while reducing costs associated with substrate procurement[23].

Pure cultures, particularly *Clostridium* species, have demonstrated higher hydrogen yields due to their specific metabolic capabilities, but mixed microbial cultures are often utilized[24]19/11/2024 22:39:00. These, such as those derived from sewage sludge, offer greater resilience to environmental fluctuations, including changes in substrate availability, pH, and temperature[25]. However, they raise a critical aspect in dark fermentation which is the possible reduction in hydrogen production due to the presence of homoacetogenic bacteria[25]. These anaerobic microorganisms consume hydrogen and carbon dioxide to produce acetic acid, thus decreasing the net amount of hydrogen produced. Homoacetogens are ubiquitous in mixed cultures and can adapt to different operating conditions, making their complete elimination difficult[26].

Understanding and controlling homoacetogenesis is crucial to optimize hydrogen production by dark fermentation. Studies have shown that homoacetogenesis can consume 11% to 43% of the hydrogen produced in single or repeated batch fermentations[25]. However, the precise quantification and dynamics of this phenomenon during continuous fermentations remain poorly understood[25].

Strategies to mitigate the effect of homoacetogens include controlling operating conditions, such as pH and CO₂ concentration, and using models that incorporate thermodynamic and kinetic controls to predict the dynamics of homoacetogenesis[27]19/11/2024 22:39:00. The implementation of advanced techniques, such as radioactive tagging, could provide detailed information on the simultaneous production and consumption of hydrogen during fermentation[25].

To transition dark fermentation technology from laboratory research to industrial or commercial applications, it is bottom-line to model, calibrate, and optimize the process. Researchers have predominantly adapted existing mathematical models to describe experimental results, with the empirical Gompertz model and the Anaerobic Digestion Model No. 1 (ADM1) of the International Water Association (IWA) being among the most frequently used[28], [29].

The Gompertz model, based on a sigmoid function applied to time-series data, is commonly employed to estimate the maximum potential for hydrogen production and determine the lag phase. However, it has limitations in interpreting process kinetics because it excludes critical operating conditions such as substrate type and concentration, pH, temperature, and partial gas pressure that govern the fermentation reaction[28], [30].

ADM1, in contrast, is a comprehensive kinetic model based on Monod-type equations, extensively used to model anaerobic digestion processes [31], [32]. In recent years, researchers have adapted ADM1 to model dark fermentation reactions by estimating kinetic parameters through batch and continuous experiments using Monod or Michaelis–Menten kinetics[28]. Nevertheless, ADM1 requires modifications to accurately describe non-methanogenic systems, often relying on constant stoichiometry to represent product generation from carbohydrate fermentation[28], [33].

Despite these advancements, biological hydrogen production remains inherently unstable and unpredictable, heavily dependent on fermentation conditions such as pH, hydraulic or solid retention time, hydrogen partial pressure, acid concentration, the presence of methanogenic microorganisms, and the microbial communities of hydrogen-producing bacteria[34], [35]. Although it is known there are species that predominate in hydrogen fermentation processes, their precise quantitative contribution to hydrogen production has yet to be clearly identified[36], [37], [38].

There remains a lack of robust paradigms that combine advanced computational techniques to model key metabolic intermediates during dark fermentation for biohydrogen production. To start addressing this gap, the article proposes developing a model based on the combination of the kinetics of three main reactions: the acetate pathway, the butyrate pathway, and homoacetogenesis. Including homoacetogenesis is particularly novel, as this process can consume a significant proportion of the hydrogen produced, thereby reducing the overall efficiency of the process.

The objective of this study is to develop an advanced kinetic model that integrates homoacetogenesis to enhance the accuracy of hydrogen production prediction during dark fermentation. By improving the model's predictive capabilities, this approach is expected to facilitate the optimization of operating conditions and to support the development of effective strategies to control the influence of homoacetogens on hydrogen yields. Such advancements in modeling are anticipated to significantly contribute to the field of biological hydrogen production, facilitating its scalability to industrial applications.

2. Materials and Methods

2.1 Experiments

The dark fermentation experiments supporting the development of the model were conducted by the research group using six different setups. The general characteristics and conditions common to all setups are presented first, followed by detailed descriptions of the specific reactor volumes and operational conditions for each setup.

The inoculum was composed of cattle manure (4% VS) sourced from local Danish farms that was pre-treated thermally (12°C for 30 min) and with acidification (buffer agent: H₂SO₄) to inhibit hydrogen-consuming bacteria. The slurry samples, used as the starting material for fermentation, consisted of a mixture of mainly cattle manure and either biopulp or glucose as the substrate. The biopulp, supplied by the Danish company Biofos, is derived from food waste and is characterized in Table 1.

	TS [%]	VS [%]	COD [g/L]	TKN [mg/L]	Sugars [g/L]
Average	15	13	71.05	0.803	95.11
STD	0.4	0.3	0.99	0.006	34.54

Table 1: Detailed characterization of biopulp feedstock

Nitrogen sparging was conducted by purging pure nitrogen gas into the slurry samples at a controlled overpressure of 0.75 - 1 bar to capture volatile fatty acids (VFA) and other condensable gases. The exiting gas, rich in VFA and moisture, was directed through a trap where VFAs and condensable gases were accumulated. A vent system released any immiscible gases to prevent headspace buildup, ensuring accurate analysis of VFA content.

VFA in the slurry samples were analyzed using gas chromatography (GC) specifically configured to identify and quantify VFAs, mainly acetic acid and butyric acid.

The pH of the samples was measured using a pH meter to monitor and potentially control the reactor conditions. GC was utilized to measure the concentrations of carbon dioxide (CO₂) and hydrogen (H₂) in the gas phase, providing critical data on the gaseous by-products of the reaction.

2.1.1 Batch Experiments

Five batch fermentation tests (Experiments 1–5) were performed to investigate hydrogen production under varying initial pH conditions and substrate types. The initial concentrations of organic acids - specifically acetic and butyric acid - were measured for each experiment to establish consistent starting conditions. In all experiments, the initial concentrations of acetic acid and butyric acid in the starting medium were approximately 0.394 and 0.180 mol/L, respectively, with slight variations around these values.

In Experiments 1 and 2, 2 g of glucose were dissolved in water to prepare the culture medium and to achieve a reactive volume of 40 mL in a 118 mL serum bottle. Dissolved oxygen was removed by sparging the medium with nitrogen gas to establish anaerobic conditions. The initial pH for Exp. 1 was measured to be 5.0, while for Exp. 2 it was adjusted to 7.0. Differently, Exp. 3 used biopulp instead of glucose, maintaining the same volatile solids amount, i.e. 2 gVS, and the same working volume as in Exp. 1 and 2. The initial pH for Exp. 3 was also adjusted to 7.0 [39], [40]. The pH was varied to investigate its potential effects on hydrogen production, with no pH control strategy being implemented.

All serum bottles were inoculated, sealed, and kept in an incubator at 55 °C. Exp. 1 was carried out for 98 days, Exp. 2 for 63 days, as no further changes in production were observed, and Experiment 3 for 98 days. Throughout these experiments, only hydrogen gas production was measured. Gas samples were collected periodically and analyzed for hydrogen content using GC.

In Experiments 4 and 5, 2 g of glucose were dissolved in water to prepare the culture medium, achieving a working volume of 25 mL in 75 mL serum bottles. Dissolved oxygen was removed by sparging with nitrogen. The initial pH was adjusted to 7.0 for Experiment 4 and to 10.0 for Experiment 5. The bottles were inoculated, sealed, and incubated at 55 °C for 20 days without pH control. In these experiments, both hydrogen and carbon dioxide production were measured. Gas samples were collected at regular intervals and analyzed for hydrogen and carbon dioxide concentrations using GC.

2.1.2 Continuous Experiment

Experiment 6 was conducted using a 1 L continuously stirred tank reactor (CSTR) to evaluate hydrogen production under continuous operation with varying influent substrate concentrations. Half-filled with the reactive fluid, the bottle was heated with a heating jacket at a temperature of 55°C and it was operated atmospheric pressure, with continuous stirring to maintain homogeneity. Dissolved oxygen was removed by sparging the medium with nitrogen gas. The initial pH was

adjusted to 5.5 using 1 M NaOH as a buffer agent, as previous experimental results indicated this to be the optimal value [41].

An influent flow rate of 25 mL/day was maintained during the whole 100 days, and the effluent flow was adjusted to keep the working volume constant, resulting in a hydraulic retention time of 20 days. The glucose concentration in the influent was increased stepwise: 5 g/L from days 1 to 3, 10 g/L from days 4 to 8, 15 g/L from days 9 to 13, 20 g/L from days 14 to 23, 25 g/L from days 24 to 43, 30 g/L from days 44 to 64, and 35 g/L from day 65 until the end of the 100-day experiment. This corresponded to an OLR range of 0.25 – 1.75 gVS/L/d

A 1 M NaOH solution was added periodically to maintain the pH above inhibitory levels to compensate for acidification due to organic acid production. The pH was monitored daily using a calibrated pH meter, and adjustments were made when necessary.

Hydrogen, carbon dioxide, and organic acids (acetic acid and butyric acid) were measured. Gas samples were collected daily and analyzed for hydrogen and carbon dioxide concentrations using gas chromatography. Liquid samples were taken periodically to measure how concentrations changed over time.

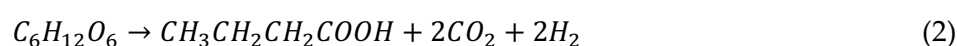
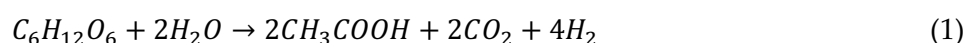
2.2 Mathematical Modeling

2.2.1 Metabolic Pathway and Kinetic Modeling

Dark fermentation takes place in several stages. Initially, enzymatic hydrolysis breaks down the high molecular weight organic compounds into water-soluble substances, such as glucose[42]. These simpler compounds are then metabolized by bacteria to produce volatile fatty acids (VFAs), hydrogen, and carbon dioxide[43]. The accumulation of VFAs and other byproducts can inhibit microbial activity and reduce hydrogen yields, presenting a challenge to the efficiency of the process[44].

Dark fermentation is adaptable to various environmental conditions through adjustments in pH, temperature, organic loading rate (OLR), and hydraulic retention time (HRT), allowing optimization across different operational settings[45]. Microorganisms involved include *Clostridium* and *Enterobacter* genera, such as *Clostridium Butyricum*, *Clostridium Beijerinckii*, *Enterobacter Asburiae*, and *Enterobacter Eerogenes*. These bacteria utilize metabolic pathways involving hydrogenase and nitrogenase enzymes to produce hydrogen [46], [47].

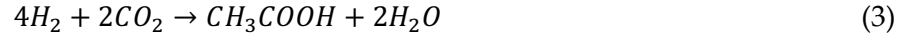
The theoretical maximum hydrogen yield is 4 moles of H₂ per mole of glucose via the acetate pathway and 2 moles via the butyrate pathway as represented by (1 and (2 below [48].



However, in practice, yields range from 0.1 to 3.8 moles of H₂ per mole of hexose, influenced by operating conditions and microbial strains employed in the process and the simultaneous production of other metabolites, such as butyric acid. Substrate type, temperature, pH, and inoculum percentage significantly impact hydrogen production efficiency[49]. Optimal pH levels are critical for hydrogenase activity, with different studies reporting varying optimal values[50].

A mathematical model has been developed to simulate hydrogen production during dark fermentation while analyzing the underlying kinetics. The model integrates the main metabolic pathways involved in the process, particularly those characterizing the acidogenesis phase, which is essential to account for hydrogen production. Simultaneously, it also accounts for homoacetogenesis, a parallel metabolic pathway recognized during this process.

Homoacetogenesis consumes molecular hydrogen and carbon dioxide to produce additional acetic acid, as shown in **Error! Reference source not found.**:



The correlation between the specific rate of substrate consumption and substrate concentration is expressed through the Michaelis-Menten kinetics [51]. This relationship is appropriate when the concentration of a single substrate (S) limits the degradation rate while the accumulation of growth-inhibiting compounds is negligible [51]. The equation states as follows ((4):

$$r_1 = K_{g,max} \left(\frac{S}{K_s + S} \right) X I_{pH} \quad (4)$$

Where $K_{g,max}$ is the maximum specific uptake rate (1/day), S represents the mol of substrate in the system, K_s is the saturation constant (mol), X is the amount of microorganisms present in the system (mol) and I_{pH} is a function accounting for the inhibition from pH based on previous findings [52]. The function is listed below ((5):

$$I_{pH} = \exp \left(-3 \left(\frac{pH - pH_u}{pH_u - pH_l} \right)^2 \right) \quad (5)$$

Where pH is the value of pH referring to the system which is calculated through a charge balance using the equation below ((6) while pH_u and pH_l are the upper and the lower limits of the optimal pH range, set at 10 and 3.5, respectively.

The charge balance expressed in (6:

$$H^+ + S_{in} = Ac^- + Bu^- + HCO_3^- + OH^- \quad (6)$$

considers all ionic species present in solution, including hydrogen ions [H^+], inorganic positive species, such as Na^+ or K^+ , that might be present at the beginning [S_{in}], the anions resulting from the dissociation of organic acids ($[Ac^-]$ for acetic acid and $[Bu^-]$ for butyric acid), bicarbonate [HCO_3^-] and hydroxide ions [OH^-], as previously presented [52]. The acid dissociation constants are used to calculate the concentrations of the ionized forms of the respective species. The charge balance equation is then solved iteratively to find the concentration of [H^+], from which is derived the pH.

The rate of hydrogen consumption by homoacetogenic bacteria, denoted as r_2 , is modeled through (7 assuming a Michaelis-Menten kinetic for this reaction as well:

$$r_2 = \lambda(t) K_{H_2,max} \left(\frac{H_2}{K_{s,H_2} + H_2} \right) X I_{pH} I_{H_2} \quad (7)$$

where $K_{H_2, \max}$ is the maximum hydrogen consumption rate (1/day) and K_{S, H_2} is the half-saturation constant (mol), reflecting the enzymes' affinity for available hydrogen. I_{pH} is the same function included in r_1 accounting for pH inhibition.

In this expression, $\lambda(t)$ represents the homoacetogenesis activation function, describing the delayed initiation of this process over time and considering the adaptation period of homoacetogenic bacteria, expressed by the parameter t_{shift} , as shown below ((8). Specifically, it was assumed to behave as a sigmoidal function:

$$\lambda(t) = 1 / \left(1 + \exp \left(- \frac{(t - t_{shift})}{5} \right) \right) \quad (8)$$

$$I_{H_2} = \frac{K_{i, H_2}}{K_{i, H_2} + H_2} \quad (9)$$

The hydrogen inhibition function shown in (9) was introduced into the model to attempt to provide a preliminary representation of the inhibitory effect of high concentrations of hydrogen on homoacetogenesis. This experimental approach constitutes an attempt to model a complex phenomenon, recognizing that further studies are necessary for a more accurate characterization of hydrogen inhibition.

Once the two main reaction rates of the system, r_1 , and r_2 , were defined, the dynamics of the concentrations of the different species involved in the process can be described using a system of ordinary differential equations (ODE). These equations are based on the three fundamental reactions considered in the process and incorporate experimentally determined stoichiometric coefficients, which represent the fractions of substrate converted into each product and the proportions in which the species are consumed or produced in the reactions. The coefficients related to hydrogen production in the acetate and butyrate pathways will henceforth be referred to as f_i , while those associated with hydrogen consumption in the homoacetogenesis pathway will be referred to as a_i , as shown in in Eq. (10 - (15 [29].

Based on the three reactions considered, it is possible to formulate the ODEs that describe the temporal evolution of the concentrations of the species in the system represented in Eq. (10 - (15 [29]:

$$\frac{dS}{dt} = -r_1 \quad (10)$$

$$\frac{dX}{dt} = Yr_1 - k_d X \quad (11)$$

$$\frac{dH_2}{dt} = (1 - Y)f_{H_2}r_1 - \alpha_{H_2}r_2 \quad (12)$$

$$\frac{dHAc}{dt} = (1 - Y)f_{HAc}r_1 + \alpha_{HAc}r_2 \quad (13)$$

$$\frac{dHAb}{dt} = (1 - Y)f_{HAb}r_1 \quad (14)$$

$$\frac{dCO_2}{dt} = (1 - Y)f_{CO_2}r_1 - \alpha_{CO_2}r_2 \quad (15)$$

Where S is the substrate [mol], X indicates the biomass [mol], Y represents the yield of substrate conversion into biomass defined as the moles of biomass produced per mole of substrate consumed and k_d is the biomass decay constant [1/day]. The f_i coefficients represent the experimental stoichiometric coefficients associated with the acidogenesis phase, while the α_i coefficients refer to the homoacetogenesis phase.

2.2.2 Numerical Integration

The system of differential equations is numerically integrated using SciPy's *solve_ivp* function, which implements the LSODA algorithm [53]

This method is suitable for rigid and non-rigid systems and allows accurate control of integration tolerances. Integration is performed in the time domain of interest, which covers the duration of the experiment or process to be modeled.

2.2.3 Parameters Estimation and Modeling

An optimization of parameters was performed to fit the model to the experimental data, using the L-BFGS-B algorithm via SciPy's *minimize* function. The objective function to be minimized is the root mean square error (RMSE) between the model predictions and the experimental hydrogen production data.

3. Results and Discussion

3.1 Comparison Between Model Predictions and Experimental Data

This section reports the results of the comparison between the six experiments and the model predictions to assess the accuracy of the simulations and to analyze any discrepancies between them. The experiments differed not only in their operating conditions, but also in the experimental data collected: some provided measurements of hydrogen only, others of hydrogen and carbon dioxide, while in the last case, data on pH and organic acids were also collected. These differences were attributed to the specific objectives of the experiments: the first aimed solely at accounting for hydrogen production, the second focused on the influence of pH on the purity and productivity of the reactors and the last examined the effect of glucose concentration on the system's yield.

3.1.1 Analysis of Batch Experiments from 1 to 3

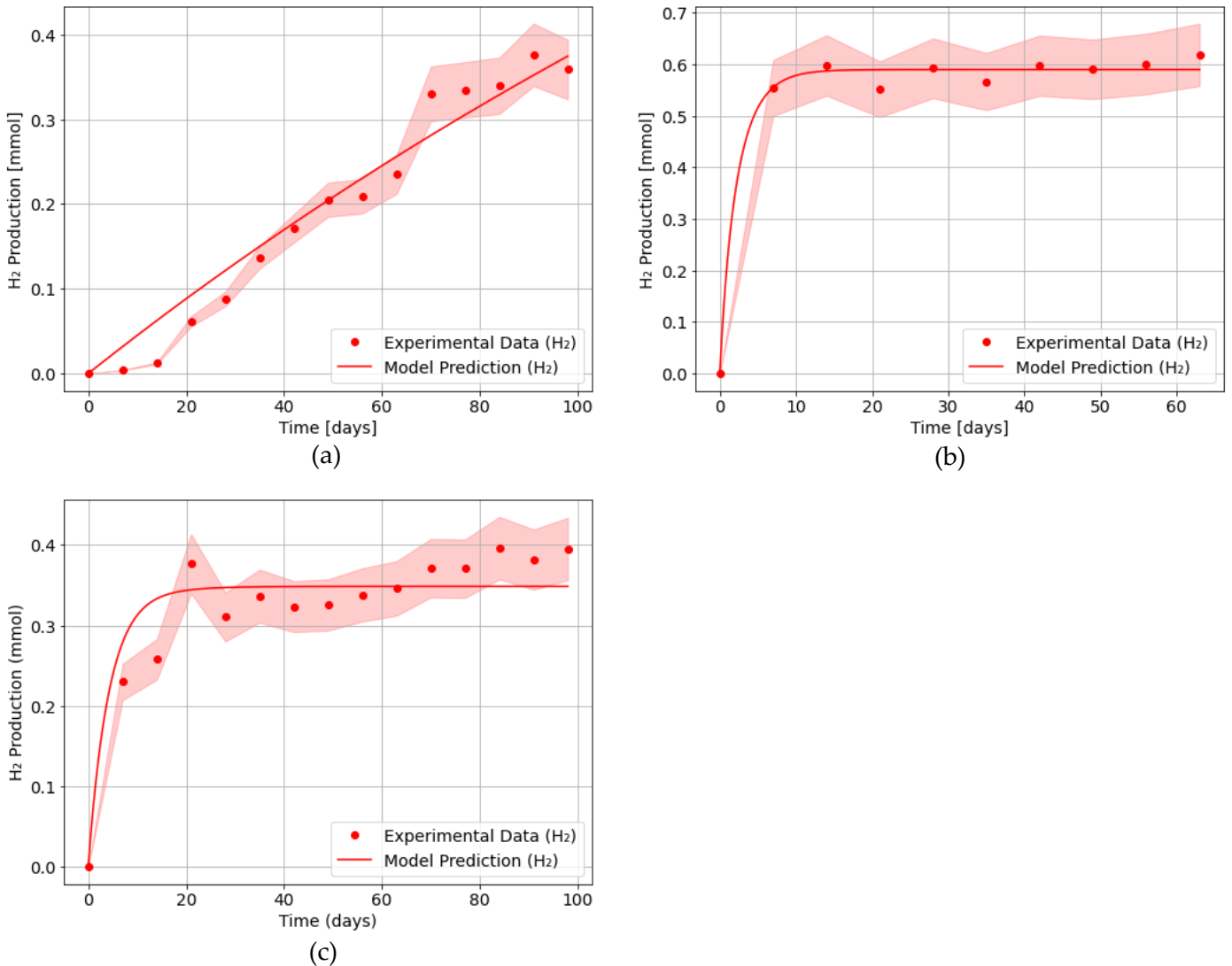


Figure 1: Hydrogen production (mmol) over time (days) for Experiment 1 (a), Experiment 2 (b) and Experiment 3 (c), with a 5% uncertainty band included to represent measurement variability.

In the first three batch experiments, the experimental data concerned only hydrogen production. As shown in Fig. 1 the comparison between experimental data and model predictions indicates a satisfactory accuracy. This has been also demonstrated by the R^2 values, which are 0.959 for Experiment 1 (Figure 1a), 0.990 for Experiment 2 (Figure 1b), and 0.868 for Experiment 3 (Figure 1c), reflecting a great agreement between the model result and the experimental data. In these experiments, the pH and substrate type were varied to assess their impact on the outcomes. Specifically, the pH was not controlled in Experiment 1, where only the inoculum was used, while in Experiments 2 and 3, pH was initially adjusted to 7, and the substrate used was pure glucose and biopulp, respectively. Remarkably, the concentration of volatile solids was maintained constant across all experiments, at 2 g/L.

Comparing the results of the Experiments 1 and 2, it can be observed that in Experiment 1, there is a noticeable delay in the onset of hydrogen production, and the final productivity is lower compared

to Experiment 2. These differences are likely due to reduced microbial activity caused by sub-optimal pH levels.

A comparison between Experiment 2 and Experiment 3 reveals a similar trend, with a rapid initial substrate consumption followed by stabilization, leading to a plateau. Nevertheless, the plateau observed in Experiment 3 is lower than that in Experiment 2, resulting in reduced hydrogen production. This discrepancy can be attributed to differences in substrate accessibility: while glucose in Experiment 2 provided a readily assimilable carbon source for microorganisms, the biopulp used in Experiment 3, being a more complex substrate, limited the degradation rate and nutrient availability, thereby reducing the overall efficiency of hydrogen production[39], [40].

The lower initial slope of hydrogen production in Experiment 3 can similarly be attributed to the reduced substrate accessibility, likely slowing microbial activity during the initial stages, consuming energy breaking down the organic matter, and thus limiting the hydrogen production rate compared to glucose. The small peak observed around day 20 may indicate microbial adaptation or a sudden increase in substrate availability, temporarily accelerating the fermentation process before returning to a more stable but lower hydrogen production rate due to the subsequent reduction of glucose in the liquid.

These results are consistent with what has been reported in the literature regarding the variability in the efficiency of anaerobic fermentation depending on the type of substrate used[49], [54]. More complex substrates such as biopulp require longer degradation times, negatively affecting both the initial rate of hydrogen production and the total amount produced[55].

3.1.2 Analysis of Batch Experiments 4 and 5

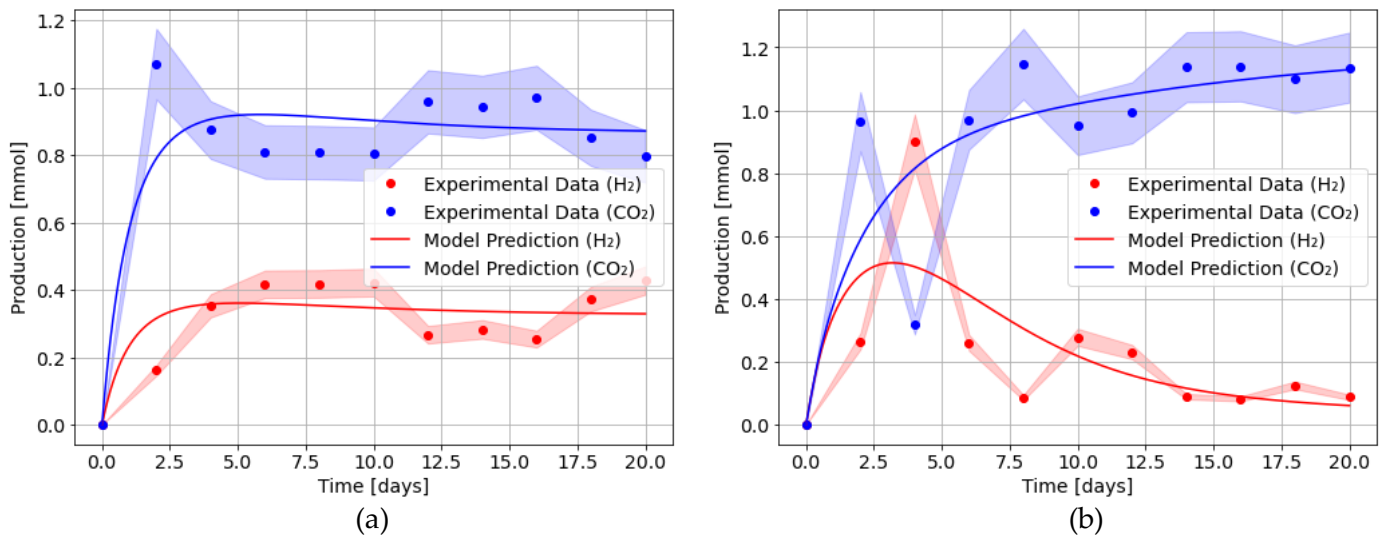


Figure 2: Hydrogen production (mmol) over time (days) for Experiment 4 (a) and Experiment 5 (b), with a 5% uncertainty band included to represent measurement variability.

In Experiment 4 (Figure 2a) and 5 (Figure 2b), data on carbon dioxide were also collected other than hydrogen. These two experiments differed only on the initial pH setting: in Experiment 4 the pH was set to 7, while in Experiment 5 it was set to 10. In both cases, glucose was chosen as the substrate. The results obtained are shown in Figure 2.

Although the accuracy was lower than in previous cases, as reflected by the R^2 values of 0.65 and 0.83 in Experiment 4, and 0.52 and 0.7 in Experiment 5, for H_2 and CO_2 respectively, the model adequately predicted the overall trends in the production of both species.

As far as hydrogen production is concerned, although the maximum peak is reached when the experiment is conducted at a pH of 10, with a value of 0.9 mmol as opposed to 0.43 mmol in the case of pH 7, the total overall production is higher in Experiment 4. This indicates that a pH of around 7 is more favorable for sustained hydrogen production.

In contrast to Experiments 1-3, in these two cases, a H_2 descending phase was observed after an initial peak. This pattern in the hydrogen production, not present in experiments 1-3, suggests that the model may not account for the phenomenon causing this behavior, leading to lower R^2 values. The observed trend could be attributed to a possible change in the microbial community, which caused a momentary decrease in the activity related to hydrogen production or could indicate the activation of hydrogen consumption mechanisms, towards mechanisms of homoacetogenesis [56] [25].

With regard to CO_2 production, the model showed good predictive ability, suggesting that the processes governing its production were adequately captured.

3.1.3 Analysis of the Continuous Experiment

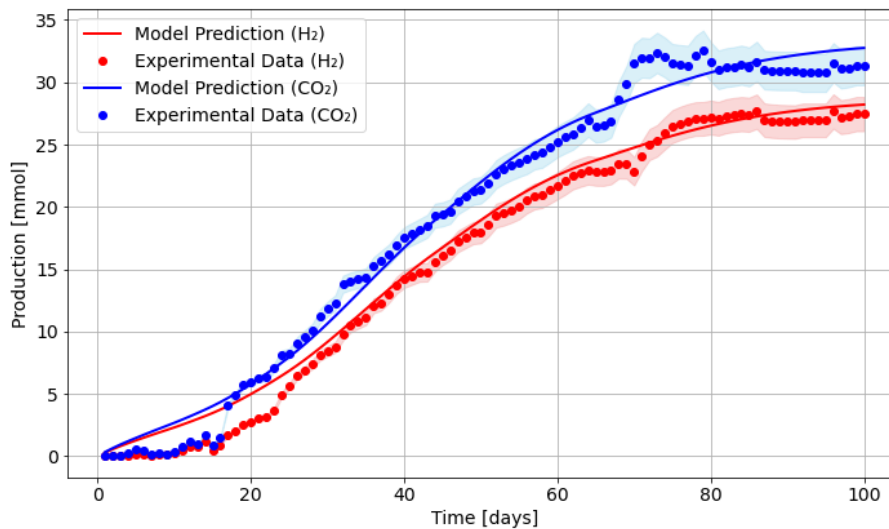


Figure 3: Hydrogen and Carbon Dioxide production (mmol) over time (days) for Experiment 6, with a 5% uncertainty band included to represent measurement variability.

Finally, as shown in Figure 3, the model successfully captured the CSTR system dynamics, accurately simulating the H_2 and CO_2 trends. The R^2 values were 0.986 and 0.987, respectively, indicating great accuracy. Although this had minimal impact on the overall R^2 value, in the initial phase, the model slightly overestimated hydrogen and carbon dioxide production, likely due to the absence of a lag phase, which could be more significant under continuous operation. Despite this, both gases displayed a clear increasing trend, stabilizing at a plateau after around 70 days. Before reaching the plateau, a simultaneous very small decrease in the production of both gases is observed, which may indicate a shift in the microbial community[56].

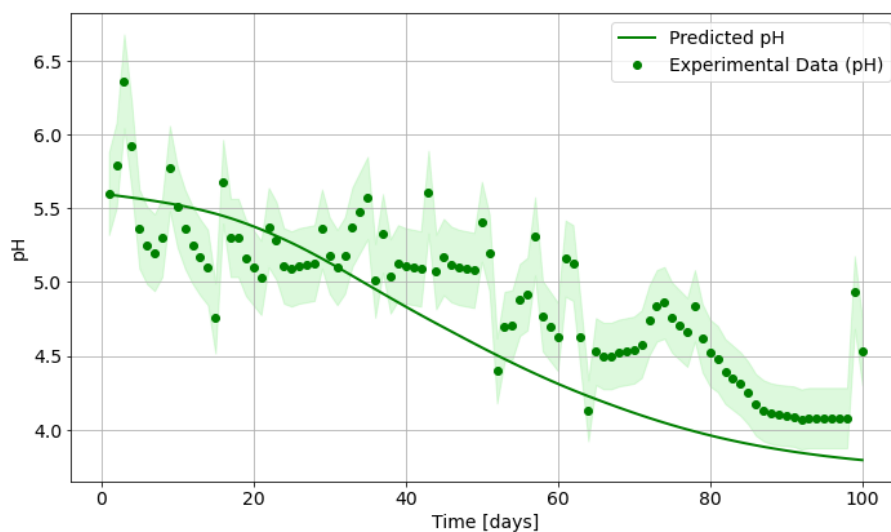


Figure 4: pH evolution over time (days), with a 5% uncertainty band included to represent measurement variability.

As represented in Figure 4, the model also captured the overall pH trend, though a lower R^2 suggests some fluctuations were not fully accounted for, indicating areas for further refinement in the model.

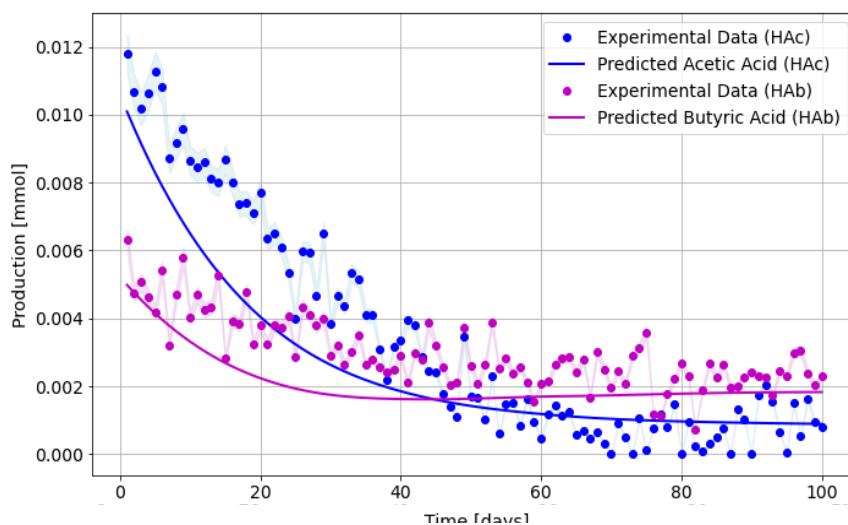


Figure 5: Production of acetic acid and butyric acid (mmol) over time (days), with a 5% uncertainty band included to represent measurement variability.

As predictable, given the observations regarding pH accuracy and the fact that organic acids are the primary drivers of these pH changes, the model also demonstrated reduced accuracy in predicting organic acids production, as shown in Figure 5. This could be also due to the limited and irregularly distributed experimental data collected, precisely eight data points were available over 100 days, and then a polynomial regression analysis was conducted.

Despite this, the model offers a useful qualitative representation, both for pH and organic acids.

3.2 Model Key Parameters Discussion

This section presents the key parameters obtained from the analysis of the six datasets considered in this study, which are essential for understanding the system's dynamics and the influence of operating conditions.

The parameters were analyzed in relation to the operating conditions varying between datasets, focusing on three main variables: operation time (days), total reactor volume (mL), initial pH value (pH₀), and substrate type. The variables for the six experiments are summarized in Table 2:

	Exp. 1	Exp. 2	Exp. 3	Exp. 4	Exp. 5	Exp. 6
Residence Time [days]	98	63	98	20	20	20
Reactive Volume [ml]	40	40	40	25	25	500
pH₀	5	7	7	7	10	5.6
pH control	no	no	no	no	no	yes
Substrate Type	glucose	glucose	biopulp	glucose	glucose	glucose

Table 2: Table summarizing most relevant operating conditions across six experiments

The values obtained for the parameters through the regression are summarized in Table Table 3 - Table 4:

	Y [mol _{biomass} / mol _{substrate}]	K_d [1/day]	$K_{g,max}$ [1/day]	K_{s1} [mol]	f_{HAc}	f_{HAb}	f_{H_2}	f_{CO_2}
Exp. 1	0.188	0.002	0.20	4.9	0.76	0.35	1.2	0.9
Exp. 2	0.310	0.242	5.6	1.3	0.61	0.21	0.13	0.9
Exp. 3	0.152	0.141	5.0	3.5	0.51	0.30	0.11	0.7
Exp. 4	0.744	0.220	5.1	0.73	0.61	0.21	0.15	0.4
Exp. 5	0.726	0.057	6.1	2.0	0.65	0.33	0.50	0.9
Exp. 6	0.890	0.001	5.6	0.55	0.1	0.22	3.5	4

Table 3: Kinetic parameters for biomass evolution and for hydrogen production pathways

	t_{shift} [day]	$K_{\text{H}_2, \text{max}}$ [1/day]	K_{s, H_2} [mol]	K_{i, H_2} [mol]	a_{H_2}	a_{HAc}	a_{CO_2}
Exp. 1	7.8	3.5	3.3	0.5	4.9	0.76	0.35
Exp. 2	8.0	4.0	2.5	0.5	1.3	0.61	0.21
Exp. 3	8.0	4.0	2.6	0.3	3.5	0.51	0.30
Exp. 4	8.0	3.9	2.6	0.5	0.73	0.61	0.21
Exp. 5	7.8	4.8	0.5	0.5	2.0	0.65	0.33
Exp. 6	93	1.6	9.8	1e-4	0.55	0.1	0.22

Table 4: Kinetic parameters obtained for the homoacetogenesis pathway

The Michaelis-Menten kinetics for glucose consumption is described by $K_{\text{G}, \text{max}}$ and K_{s} , representing the maximum microbial growth rate and the glucose saturation constant. To assess microbial efficiency in glucose utilization, k_{d} and Y were determined, with Y reflecting the biomass yield and k_{d} the biomass decay constant. The metabolic pathways of acetate and butyrate were analyzed through stoichiometric coefficients f_{HAc} , f_{HAB} , and f_{CO_2} . For homoacetogenesis kinetics, $K_{\text{H}_2, \text{max}}$ and K_{s, H_2} represent the maximum hydrogen consumption rate and the hydrogen saturation constant. Additionally, the time shift t_{s} , X_0 and K_{i, H_2} were determined to account for microbial adaptation time, initial biomass concentration, and hydrogen inhibition. Finally, stoichiometric coefficients were also calculated to further characterize homoacetogenesis.

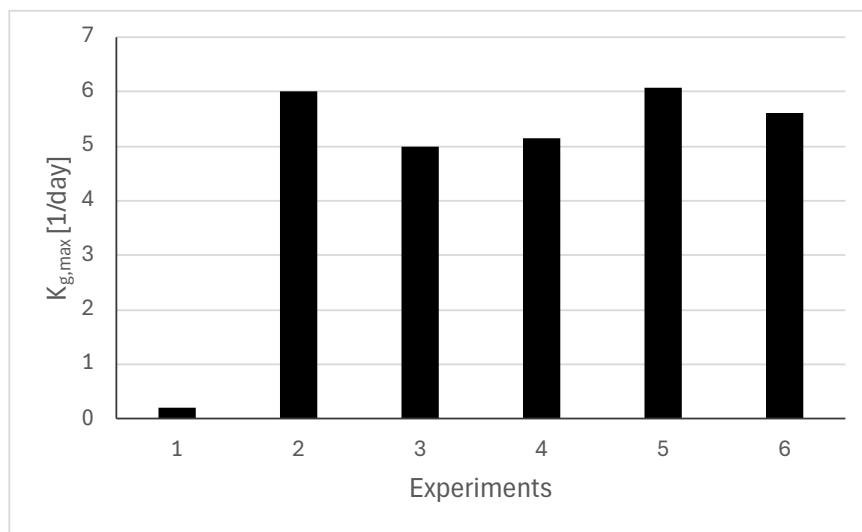


Figure 6: Bar chart illustrating the values of the constant $K_{\text{g}, \text{max}}$ (1/day) across six experiments

As the graph shows (Figure 6), the *quasi*-constant value of $K_{g,max}$ around 5.5 1/day suggests an intrinsic dependence on the biological characteristics of the microorganisms and the nature of the process, fixing the value in the various experiments. A significant reduction in its value can be observed in the first experiment, likely due to the particularly low initial pH, which was the lowest among all experiments and was not adjusted during the experimental procedure.

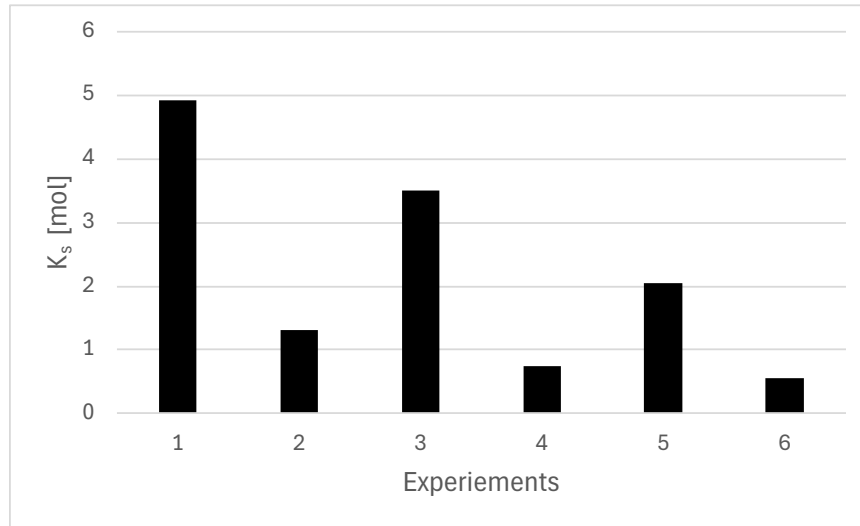


Figure 7: Bar chart illustrating the values of the constant K_s (mol) across six experiment

Error! Reference source not found. shows the values obtained for the saturation constant K_s , for which no significant correlations were observed, except for a slight dependence on the ratio volume/days. However, no clear trend was identified, which suggests that further investigation is necessary to explore the potential dependency of this parameter.

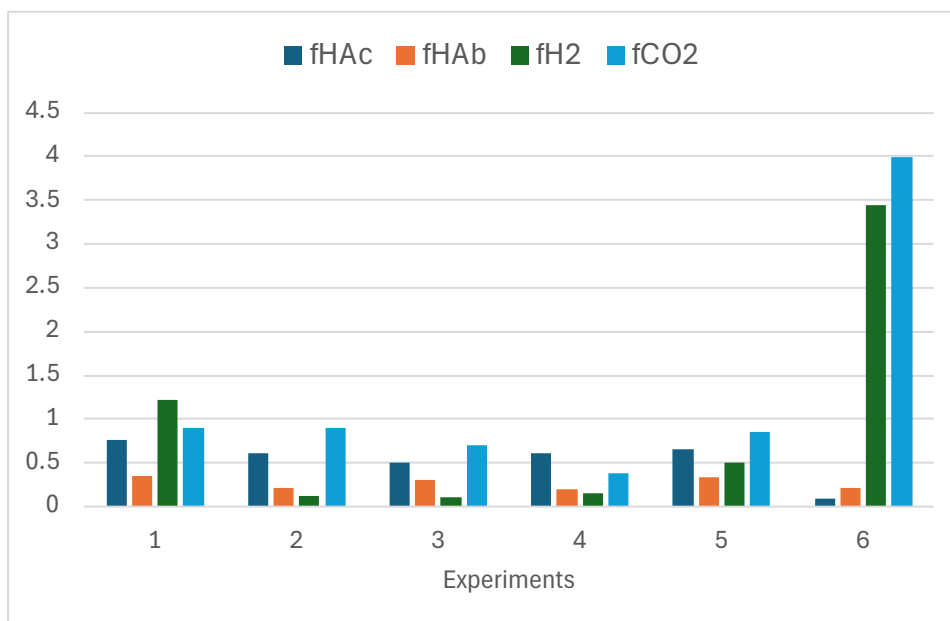


Figure 8: Bar chart illustrating the experimental stoichiometric coefficients for acetic acid (HAc), butyric acid (HAb), hydrogen (H₂) and carbon dioxide (CO₂) during the acidogenic phase across six experiments.

As for the stoichiometric coefficients accounting for the two main pathways for hydrogen production, namely the acetate pathway and the butyrate pathway, they show similar values in batch mode experiments, as depicted in **Error! Reference source not found.**. However, in continuous stirred-tank reactors (CSTR), these values differ significantly, skewing towards the production of gaseous species such as hydrogen and carbon dioxide. This trend is illustrated in **Error! Reference source not found.**. The observed higher stoichiometric coefficients for gaseous species, i.e. hydrogen and carbon dioxide, in CSTR compared to batch experiments can be explained by the dynamic environment of continuous reactors. In CSTR, the continuous addition of substrates and removal of products enhance the metabolic pathways favoring gas production. This continuous flow ensures that microorganisms are constantly supplied with fresh substrates and that inhibitory by-products are partially removed, enhancing indeed the efficiency of gas-producing pathways. In contrast, batch processes experience substrate depletion and product accumulation, which can inhibit microbial activity and reduce gas production efficiency.

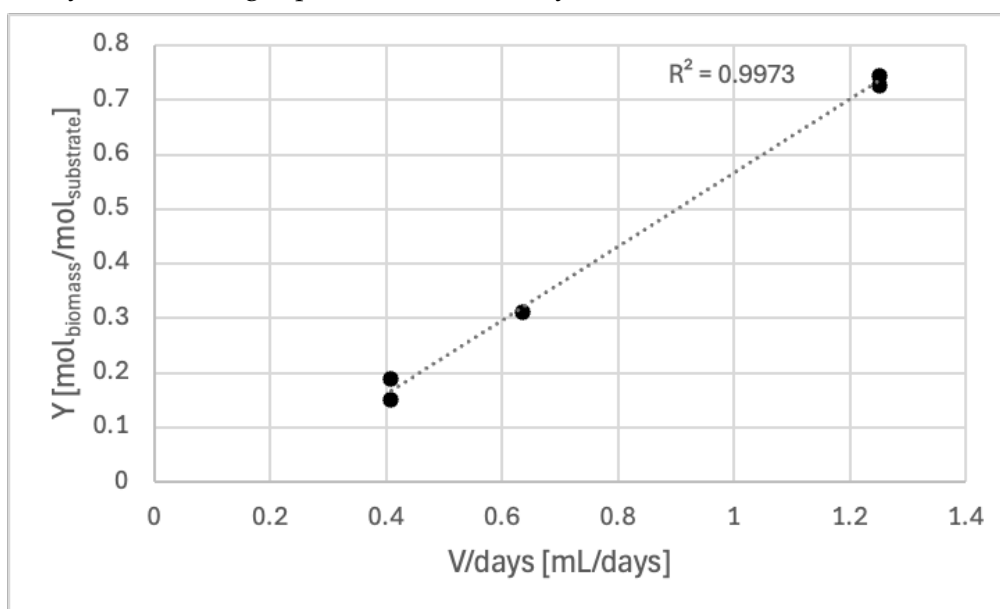


Figure 9: Graph representing the correlation between biomass yield ($\text{mol}_{\text{biomass}}/\text{mol}_{\text{substrate}}$) and the volume-to-days ratio (ml/days)

In the present study, a monotonically increasing linear relation in biomass yield is observed, in relation with the reactor volume-to-days ratio, where biomass yield is defined as the moles of biomass produced per mole of substrate consumed. In the CSTR case, the days represent the residence time, which in this case is 20. The trend is also confirmed by the R^2 coefficient of 0.99 as shown in Figure 9. The observed trend of increased biomass yield with a higher volume-to-days ratio can be attributed to the effects of the reactor volume and residence time on microbial growth and substrate utilization. Larger reactor volumes enhance the homogeneity of the culture environment, thereby improving the efficiency of substrate utilization and promoting microbial growth. Specifically, larger volumes likely reduce gradients in substrate concentrations and pH levels, both of which are critical factors influencing microbial activity [57].

Regarding residence time, biomass yield appeared to increase with decreasing residence time. This can be explained by examining dynamics of biomass growth in batch and continuous systems. In batch processes, biomass typically declines over time due to substrate depletion and the accumulation of inhibitory byproducts. In contrast, CSTRs sustain biomass growth through the

constant supply of the substrate. Therefore, especially in batch processes, as was the case in five of the six scenarios examined, extending the operation beyond optimal time frames results in prolonged periods of low biomass concentration, negatively impacting the overall yield. While this is likely true for batch systems, where glucose is rapidly consumed, leading to extended periods of substrate limitation and accumulation of acids that more readily cause inhibition and pH decrease, further investigation must be conducted for the CSTR case.

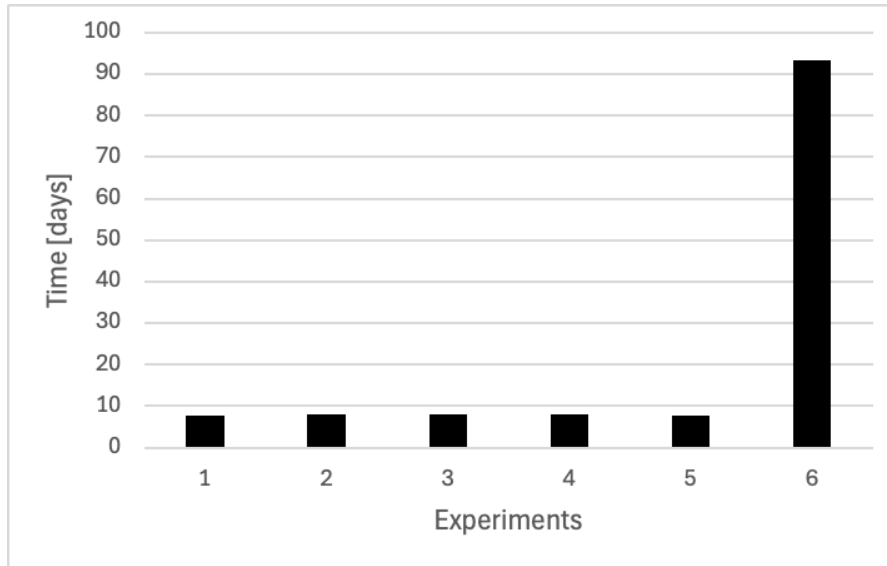


Figure 10: Bar chart depicting the lag time before the onset of homoacetogenesis

Analysis of the graph in Figure 10 shows that, in the first five Experiments, activation of homoacetogenesis occurs within the first 10 days, suggesting the presence of a potential limit in the system. However, in the last Experiment, the activation time is significantly longer, probably due to the greater and more constant supply, therefore, availability of glucose, which allows for longer hydrogen production. In support of this, it can be noted that on day 8, the residual glucose concentration is very low in the first five cases: 11, 4.2, 8.2, 1.2, and 4.6 mmol, respectively, indicating rapid substrate consumption, while in the continuous reactor it is being fed at a rate going from 0.125 g/day to 0.875 g/day. In Experiment 1, although the residual glucose is not as low as in the others, a pH below 5 may have affected metabolism, hindering hydrogen production. Therefore, the questionable data that might seem to arise from the higher residual value in case 1 can be explained by considering the inhibitory effect of the low pH. This suggests that, in addition to glucose availability, pH also plays a determining role in metabolic activity[58].

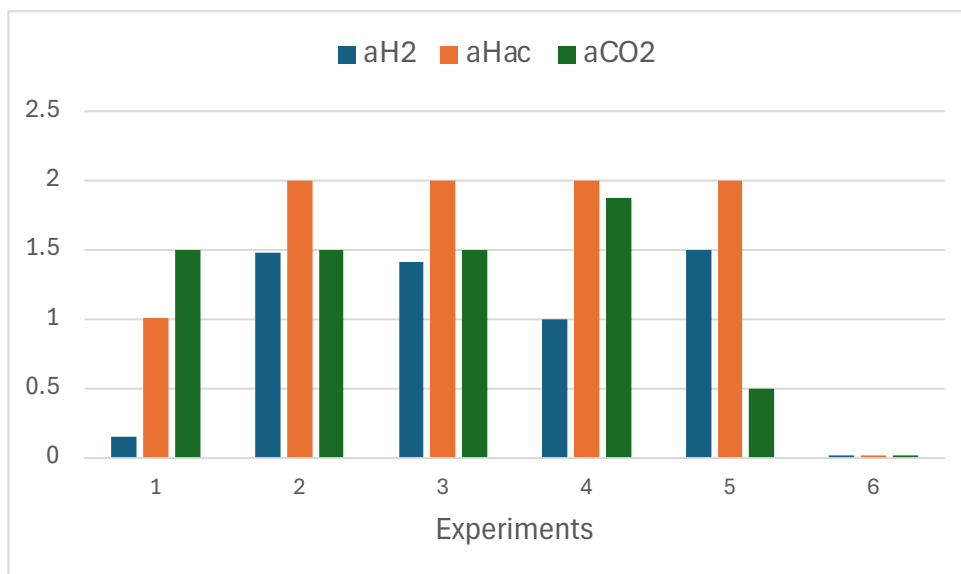


Figure 11: Bar chart illustrating the experimental stoichiometric coefficients for hydrogen (H₂), acetic acid (Hac) and carbon dioxide (CO₂) during the homoacetogenic phase across six experiments

Additionally, as shown in Figure 11, analysis of the homoacetogenesis experimental stoichiometric coefficients reveals a direct correlation with activation time: in the first five cases, where the shift is short, the coefficients are high, indicating intense homoacetogenesis activity. In contrast, in the last case, where homoacetogenesis is only activated at day 94 out of 100, the coefficients are close to zero, indicating a negligible impact of this metabolic process. This trend shows that homoacetogenesis plays a predominant role in cases of rapid activation, while it is insignificant when activation is late, consistent with the prolonged glucose availability observed in the last Experiment.

In Experiment 1, the lower coefficients could be explained by the lower initial production of hydrogen, which reduced the availability of this species for subsequent processes, thus limiting the intensity of homoacetogenesis.

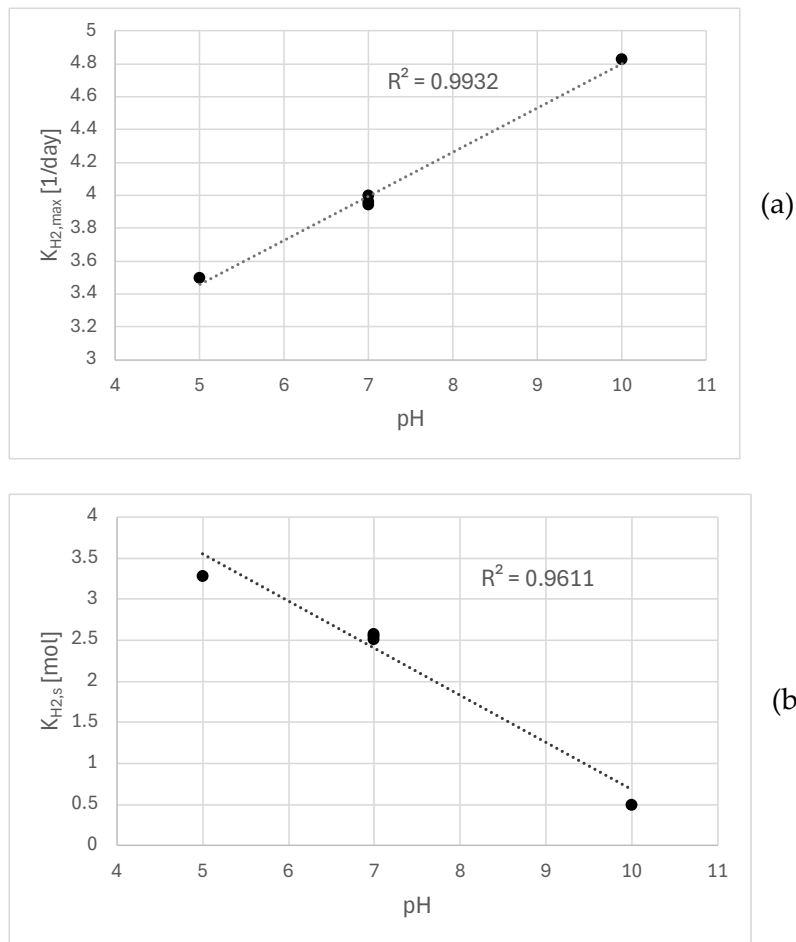


Figure 12: Graphs illustrating the correlation between the constant $K_{H_2,max}$ (a) and $K_{H_2,s}$ (b) and the pH

Regarding the kinetic constants characterizing homoacetogenesis, $K_{H_2,max}$ and $K_{H_2,s}$, as indicated in Figure 12, both exhibited a linear dependence on pH in batch experiments, although inversely. Specifically, $K_{H_2,max}$ showed an increasing trend with rising pH, whereas $K_{H_2,s}$ displayed a decreasing trend. The observed linear dependence of the kinetic constants of the two kinetic constants on pH in batch experiments can be hypothesized to result from pH-dependent enzyme activity in homoacetogenesis. As pH increases, the maximum specific hydrogen uptake rate $K_{H_2,max}$ rises, possibly due to enhanced activity of hydrogenase enzymes under alkaline conditions. Simultaneously, the decrease in the half-saturation constant $K_{H_2,s}$ suggests that the enzymes have a higher affinity for hydrogen at higher pH levels, requiring lower hydrogen concentrations to achieve half-maximal activity. This hypothesis aligns with the understanding that enzyme kinetics are influenced by pH, which affects both the activity and substrate affinity of enzymes involved in hydrogen uptake. The linear correlation has not been confirmed in the CSTR case, which may indicate that operational modes, whether continuous or discontinuous, significantly influence these parameters. Surely, further investigation in this direction is necessary for a more complete analysis.

4. Conclusions

The model developed in this study performed well, providing reliable and insightful results when compared to experimental data. The findings suggest that CSTR operation may be the most favorable mode for hydrogen production during dark fermentation, as it mitigates the negative impact of hydrogen consumption through homoacetogenesis. However, further experiments with additional CSTR cases are warranted to observe potential trends in kinetic parameters under varying operating conditions, which could offer deeper insights into optimizing this mode. Additionally, analysis of operational parameters revealed that larger reactor volumes, promoting greater homogeneity, positively influence hydrogen production, likely due to improved mixing and distribution of substrates and microorganisms.

Expanding the range of operating conditions—such as substrate type, temperature, pH, reactor volume, and fermentation duration—would allow for further refinement of the model, enhancing its predictive accuracy and adaptability to different systems.

Broadening the research to include a variety of substrates, particularly waste materials or low-value raw materials, could also improve the economic viability of the process, despite the added complexity and potential decrease in efficiency. The use of waste substrates, in particular, aligns with circular economy principles, supporting environmental sustainability and reducing costs while potentially providing an alternative to more expensive substrates like glucose.

References

- [1] J. P. Holdren, "Population and the energy problem," *Popul. Environ.*, vol. 12, no. 3, pp. 231–255, Mar. 1991, doi: 10.1007/BF01357916.
- [2] J. Wang and W. Azam, "Natural resource scarcity, fossil fuel energy consumption, and total greenhouse gas emissions in top emitting countries," *Geosci. Front.*, vol. 15, no. 2, p. 101757, Mar. 2024, doi: 10.1016/j.gsf.2023.101757.
- [3] F. Chien, H. W. Kamran, G. Albashar, and W. Iqbal, "Dynamic planning, conversion, and management strategy of different renewable energy sources: A Sustainable Solution for Severe Energy Crises in Emerging Economies," *Int. J. Hydrog. Energy*, vol. 46, no. 11, pp. 7745–7758, Feb. 2021, doi: 10.1016/j.ijhydene.2020.12.004.
- [4] A. M. Sadeq *et al.*, "Hydrogen energy systems: Technologies, trends, and future prospects," *Sci. Total Environ.*, vol. 939, p. 173622, Aug. 2024, doi: 10.1016/j.scitotenv.2024.173622.
- [5] J. B. Cristello, J. M. Yang, R. Hugo, Y. Lee, and S. S. Park, "Feasibility analysis of blending hydrogen into natural gas networks," *Int. J. Hydrog. Energy*, vol. 48, no. 46, pp. 17605–17629, May 2023, doi: 10.1016/j.ijhydene.2023.01.156.
- [6] M. Kong, S. Feng, Q. Xia, C. Chen, Z. Pan, and Z. Gao, "Investigation of Mixing Behavior of Hydrogen Blended to Natural Gas in Gas Network," *Sustainability*, vol. 13, no. 8, 2021, doi: 10.3390/su13084255.
- [7] P. E. Fixen and A. M. Johnston, "World fertilizer nutrient reserves: a view to the future," *J. Sci. Food Agric.*, vol. 92, no. 5, pp. 1001–1005, Mar. 2012, doi: 10.1002/jsfa.4532.

- [8] R. Ramachandran and R. K. Menon, "An overview of industrial uses of hydrogen," *Int. J. Hydrog. Energy*, vol. 23, no. 7, pp. 593–598, Jul. 1998, doi: 10.1016/S0360-3199(97)00112-2.
- [9] A. M. Abdalla, S. Hossain, O. B. Nisfindy, A. T. Azad, M. Dawood, and A. K. Azad, "Hydrogen production, storage, transportation and key challenges with applications: A review," *Energy Convers. Manag.*, vol. 165, pp. 602–627, Jun. 2018, doi: 10.1016/j.enconman.2018.03.088.
- [10] I. Angelidaki *et al.*, "Biogas upgrading and utilization: Current status and perspectives," *Biotechnol. Adv.*, vol. 36, no. 2, pp. 452–466, Mar. 2018, doi: 10.1016/j.biotechadv.2018.01.011.
- [11] Z. Abdin, A. Zafaranloo, A. Rafiee, W. Mérida, W. Lipiński, and K. R. Khalilpour, "Hydrogen as an energy vector," *Renew. Sustain. Energy Rev.*, vol. 120, p. 109620, Mar. 2020, doi: 10.1016/j.rser.2019.109620.
- [12] Z. Guellout, V. Clion, Y. Benguerba, C. Dumas, and B. Ernst, "Study of the dark fermentative hydrogen production using modified ADM1 models," *Biochem. Eng. J.*, vol. 132, pp. 9–19, Apr. 2018, doi: 10.1016/j.bej.2017.12.015.
- [13] A. Midilli, H. Kucuk, M. E. Topal, U. Akbulut, and I. Dincer, "A comprehensive review on hydrogen production from coal gasification: Challenges and Opportunities," *Int. J. Hydrog. Energy*, vol. 46, no. 50, pp. 25385–25412, Jul. 2021, doi: 10.1016/j.ijhydene.2021.05.088.
- [14] L. Cao *et al.*, "Biorenewable hydrogen production through biomass gasification: A review and future prospects," *Environ. Res.*, vol. 186, p. 109547, Jul. 2020, doi: 10.1016/j.envres.2020.109547.
- [15] H. Ishaq and I. Dincer, "A new energy system based on biomass gasification for hydrogen and power production," *Energy Rep.*, vol. 6, pp. 771–781, Nov. 2020, doi: 10.1016/j.egy.2020.02.019.
- [16] S. O. Jeje, T. Marazani, J. O. Obiko, and M. B. Shongwe, "Advancing the hydrogen production economy: A comprehensive review of technologies, sustainability, and future prospects," *Int. J. Hydrog. Energy*, vol. 78, pp. 642–661, Aug. 2024, doi: 10.1016/j.ijhydene.2024.06.344.
- [17] S. M. Ramu *et al.*, "Fermentative hydrogen production and bioelectricity generation from food based industrial waste: An integrative approach," *Bioresour. Technol.*, vol. 310, p. 123447, Aug. 2020, doi: 10.1016/j.biortech.2020.123447.
- [18] L. Singh and Z. A. Wahid, "Methods for enhancing bio-hydrogen production from biological process: A review," *J. Ind. Eng. Chem.*, vol. 21, pp. 70–80, Jan. 2015, doi: 10.1016/j.jiec.2014.05.035.
- [19] S. Farzad, M. A. Mandegari, and J. F. Görgens, "A critical review on biomass gasification, co-gasification, and their environmental assessments," *Biofuel Res. J.*, vol. 3, no. 4, pp. 483–495, 2016, doi: 10.18331/BRJ2016.3.4.3.
- [20] B. Reda, A. A. Elzamar, S. AlFazzani, and S. M. Ezzat, "Green hydrogen as a source of renewable energy: a step towards sustainability, an overview," *Environ. Dev. Sustain.*, May 2024, doi: 10.1007/s10668-024-04892-z.
- [21] T. C. D' Silva *et al.*, "Biohydrogen production through dark fermentation from waste biomass: Current status and future perspectives on biorefinery development," *Fuel*, vol. 350, p. 128842, Oct. 2023, doi: 10.1016/j.fuel.2023.128842.
- [22] S. Anjum *et al.*, "Bioreactors and biophoton-driven biohydrogen production strategies," *Biohydrogen Gener. Lab Ind. Chall. Perspect.*, vol. 48, no. 55, pp. 21176–21188, Jun. 2023, doi: 10.1016/j.ijhydene.2023.01.363.

- [23] C. Mahata, S. Ray, and D. Das, "Optimization of dark fermentative hydrogen production from organic wastes using acidogenic mixed consortia," *Energy Convers. Manag.*, vol. 219, p. 113047, Sep. 2020, doi: 10.1016/j.enconman.2020.113047.
- [24] J. Wang and Y. Yin, "Clostridium species for fermentative hydrogen production: An overview," *Int. J. Hydrog. Energy*, vol. 46, no. 70, pp. 34599–34625, Oct. 2021, doi: 10.1016/j.ijhydene.2021.08.052.
- [25] N. M. C. Saady, "Homoacetogenesis during hydrogen production by mixed cultures dark fermentation: Unresolved challenge," *Int. J. Hydrog. Energy*, vol. 38, no. 30, pp. 13172–13191, Oct. 2013, doi: 10.1016/j.ijhydene.2013.07.122.
- [26] M. F. Carosia, C. M. dos Reis, C. A. de Menezes, I. Kimiko. Sakamoto, M. B. A. Varesche, and E. L. Silva, "Homoacetogenesis: New insights into controlling this unsolved challenge by selecting the optimal C/N ratio, C/P ratio and hydraulic retention time," *Process Saf. Environ. Prot.*, vol. 145, pp. 273–284, Jan. 2021, doi: 10.1016/j.psep.2020.08.009.
- [27] Y. He, C. Cassarini, F. Marciano, and P. N. L. Lens, "Homoacetogenesis and solventogenesis from H₂/CO₂ by granular sludge at 25, 37 and 55 °C," *Chemosphere*, vol. 265, p. 128649, Feb. 2021, doi: 10.1016/j.chemosphere.2020.128649.
- [28] V. Gadhamshetty, Y. Arudchelvam, N. Nirmalakhandan, and D. C. Johnson, "Modeling dark fermentation for biohydrogen production: ADM1-based model vs. Gompertz model," *Int. J. Hydrog. Energy*, vol. 35, no. 2, pp. 479–490, Jan. 2010, doi: 10.1016/j.ijhydene.2009.11.007.
- [29] N. Pradhan *et al.*, "Kinetic modeling of fermentative hydrogen production by *Thermotoga neapolitana*," *Int. J. Hydrog. Energy*, vol. 41, no. 9, pp. 4931–4940, Mar. 2016, doi: 10.1016/j.ijhydene.2016.01.107.
- [30] R. Chowdhury, S. Ghosh, and P. Bhattacharya, *Bio-H₂ from Wastewater of Food Industries Using Mixed Culture: Experiments and Modelling*. 2016.
- [31] M. Sofiane *et al.*, *Modelling of dark fermentation from household organic waste based on modified ADM1*. 2013.
- [32] G. Sołowski and K. Pastuszek, "Modelling of dark fermentation of glucose and sour cabbage," *Heliyon*, vol. 7, no. 8, Aug. 2021, doi: 10.1016/j.heliyon.2021.e07690.
- [33] C. N. Economou, G. Manthos, D. Zagklis, and M. Kornaros, "ADM1-Based Modeling of Biohydrogen Production through Anaerobic Co-Digestion of Agro-Industrial Wastes in a Continuous-Flow Stirred-Tank Reactor System," *Fermentation*, vol. 10, no. 3, 2024, doi: 10.3390/fermentation10030138.
- [34] M. Niakousari, M. Razmjooei, M. Nejadmansouri, F. J. Barba, K. Marszałek, and M. Koubaa, "Current Developments in Industrial Fermentation Processes," in *Fermentation Processes*, 2021, pp. 23–96. doi: 10.1002/9781119505822.ch2.
- [35] Y. Yang *et al.*, "Enhanced thermophilic dark fermentation of hydrogen production from food waste by Fe-modified biochar," *Environ. Res.*, vol. 244, p. 117946, Mar. 2024, doi: 10.1016/j.envres.2023.117946.
- [36] E. Villanueva-Galindo, M. Vital-Jácome, and I. Moreno-Andrade, "Dark fermentation for H₂ production from food waste and novel strategies for its enhancement," *Int. J. Hydrog. Energy*, vol. 48, no. 27, pp. 9957–9970, Mar. 2023, doi: 10.1016/j.ijhydene.2022.11.339.

- [37] E. Castelló *et al.*, “Stability problems in the hydrogen production by dark fermentation: Possible causes and solutions,” *Renew. Sustain. Energy Rev.*, vol. 119, p. 109602, Nov. 2019, doi: 10.1016/j.rser.2019.109602.
- [38] Z. Y. Hitit and P. C. Hallenbeck, “Analytical procedures, data reporting and selected reference values for biological hydrogen production,” *Biomass Bioenergy*, vol. 147, p. 106014, Apr. 2021, doi: 10.1016/j.biombioe.2021.106014.
- [39] M. Alvarado-Morales, M. Kuglarz, P. Tsapekos, and I. Angelidaki, “Municipal biopulp as substrate for lactic acid production focusing on downstream processing,” *J. Environ. Chem. Eng.*, vol. 9, no. 2, p. 105136, Apr. 2021, doi: 10.1016/j.jece.2021.105136.
- [40] H. Chen, F. Xu, and Z. Li, “Solid-state production of biopulp by *Phanerochaete chrysosporium* using steam-exploded wheat straw as substrate,” *Bioresour. Technol.*, vol. 81, no. 3, pp. 261–263, Feb. 2002, doi: 10.1016/S0960-8524(01)00137-7.
- [41] D. Liu, “Bio-hydrogen production by dark fermentation from organic wastes and residues,” DTU Environment, 2008.
- [42] J. F. Soares, T. C. Confortin, I. Toderó, F. D. Mayer, and M. A. Mazutti, “Dark fermentative biohydrogen production from lignocellulosic biomass: Technological challenges and future prospects,” *Renew. Sustain. Energy Rev.*, vol. 117, p. 109484, Jan. 2020, doi: 10.1016/j.rser.2019.109484.
- [43] G. Kumar *et al.*, “A review on the conversion of volatile fatty acids to polyhydroxyalkanoates using dark fermentative effluents from hydrogen production,” *Bioresour. Technol.*, vol. 287, p. 121427, Sep. 2019, doi: 10.1016/j.biortech.2019.121427.
- [44] R. J. Jones, J. Massanet-Nicolau, A. Guwy, G. C. Premier, R. M. Dinsdale, and M. Reilly, “Removal and recovery of inhibitory volatile fatty acids from mixed acid fermentations by conventional electro dialysis,” *Bioresour. Technol.*, vol. 189, pp. 279–284, Aug. 2015, doi: 10.1016/j.biortech.2015.04.001.
- [45] M. M. Albuquerque *et al.*, “Biohydrogen Produced via Dark Fermentation: A Review,” *Methane*, vol. 3, no. 3, pp. 500–532, 2024, doi: 10.3390/methane3030029.
- [46] L. Cabrol, A. Marone, E. Tapia-Venegas, J.-P. Steyer, G. Ruiz-Filippi, and E. Trably, “Microbial ecology of fermentative hydrogen producing bioprocesses: useful insights for driving the ecosystem function,” *FEMS Microbiol. Rev.*, vol. 41, no. 2, pp. 158–181, Mar. 2017, doi: 10.1093/femsre/fuw043.
- [47] C. Hu, A. Giannis, C.-L. Chen, W. Qi, and J.-Y. Wang, “Comparative study of biohydrogen production by four dark fermentative bacteria,” *Int. J. Hydrog. Energy*, vol. 38, pp. 15686–15692, Nov. 2013, doi: 10.1016/j.ijhydene.2013.03.131.
- [48] P. K. Sarangi and S. Nanda, “Biohydrogen Production Through Dark Fermentation,” *Chem. Eng. Technol.*, vol. 43, no. 4, pp. 601–612, Apr. 2020, doi: 10.1002/ceat.201900452.
- [49] J. Wang and W. Wan, “Factors influencing fermentative hydrogen production: A review,” *Int. J. Hydrog. Energy*, vol. 34, no. 2, pp. 799–811, Jan. 2009, doi: 10.1016/j.ijhydene.2008.11.015.
- [50] M.-Y. Wang, Y.-L. Tsai, B. H. Olson, and J.-S. Chang, “Monitoring dark hydrogen fermentation performance of indigenous *Clostridium butyricum* by hydrogenase gene expression using RT-

- PCR and qPCR," *Int. J. Hydrog. Energy*, vol. 33, no. 18, pp. 4730–4738, Sep. 2008, doi: 10.1016/j.ijhydene.2008.06.048.
- [51] F. Boshagh, K. Rostami, and E. W. J. van Niel, "Application of kinetic models in dark fermentative hydrogen production—A critical review," *Int. J. Hydrog. Energy*, vol. 47, no. 52, pp. 21952–21968, Jun. 2022, doi: 10.1016/j.ijhydene.2022.05.031.
- [52] D. Batstone *et al.*, "Anaerobic digestion model No 1 (ADM1)," *Water Sci. Technol. J. Int. Assoc. Water Pollut. Res.*, vol. 45, pp. 65–73, Feb. 2002.
- [53] P. Städter, Y. Schälte, L. Schmiester, J. Hasenauer, and P. L. Stapor, "Benchmarking of numerical integration methods for ODE models of biological systems," *Sci. Rep.*, vol. 11, no. 1, p. 2696, Jan. 2021, doi: 10.1038/s41598-021-82196-2.
- [54] D.-H. Lee, "Efficiency and economic benefit of dark-fermentative biohydrogen production in Asian circular economies: Evaluation using soft-link methodology with data envelopment analysis (DEA) and computable general equilibrium model (CGE)," *2018 Asia Biohydrogen Biorefinery Symp.*, vol. 45, no. 6, pp. 3688–3698, Feb. 2020, doi: 10.1016/j.ijhydene.2019.08.250.
- [55] O. García-Depraect *et al.*, "A review on the factors influencing biohydrogen production from lactate: The key to unlocking enhanced dark fermentative processes," *Bioresour. Technol.*, vol. 324, p. 124595, Mar. 2021, doi: 10.1016/j.biortech.2020.124595.
- [56] G. Yang and J. Wang, "Changes in microbial community structure during dark fermentative hydrogen production," *Int. J. Hydrog. Energy*, vol. 44, Aug. 2019, doi: 10.1016/j.ijhydene.2019.08.039.
- [57] N. Chantawan, A. Moungrprayoon, S. Lunprom, A. Reungsang, and A. Salakkam, "High-solid dark fermentation of cassava pulp and cassava processing wastewater for hydrogen production," *ABBS-Int. Conf. Biohydrogen Bioprocesses ABBS 2020*, vol. 47, no. 96, pp. 40672–40682, Dec. 2022, doi: 10.1016/j.ijhydene.2022.09.106.
- [58] E. Ntagia, I. Chatzigiannidou, A. J. Williamson, J. B. A. Arends, and K. Rabaey, "Homoacetogenesis and microbial community composition are shaped by pH and total sulfide concentration," *Microb. Biotechnol.*, vol. 13, no. 4, pp. 1026–1038, Jul. 2020, doi: 10.1111/1751-7915.13546.